Electronic structures of $LiFePO_4$ and $FePO_4$ studied using resonant inelastic x-ray scattering

A. Hunt,[1] W.-Y. Ching,[2] Y.-M. Chiang,[3] and A. Moewes[1]
[1]*Department of Physics and Engineering Physics, University of Saskatchewan, 116 Science Place, Saskatoon, Saskatchewan, Canada S7N 5E2*
[2]*Department of Physics, University of Missouri–Kansas City, Kansas City, Missouri 64110, USA*
[3]*Department of Material Science and Engineering, Massachusetts Institute of Technology, Cambridge, Massachusetts 02139, USA*
(Received 12 September 2005; revised manuscript received 13 February 2006; published 26 May 2006)

We have studied $LiFePO_4$ and its delithiated counterpart $FePO_4$ using the resonant inelastic x-ray scattering (RIXS) and x-ray absorption techniques. Using Voigt peak fitting, we have found all unresolved RIXS transitions. These energy-loss features were then ascribed to band-to-band transitions by comparison to theoretical density of states (DOS) calculations. We have found that the DOSs of $LiFePO_4$ and $FePO_4$, as probed with the RIXS technique, agree very well with a theoretical description of the system that does not explicitly account for electron correlation effects. We propose that the interesting properties of $LiFePO_4$ result from the presence of bound magnetic polarons.

DOI: 10.1103/PhysRevB.73.205120 PACS number(s): 78.70.−g, 71.38.−k

I. INTRODUCTION

The development of cheap and reliable energy sources has always been a pressing concern for humanity in the 20th and 21st centuries. However, pollution concerns have forced energy researchers to develop technology that is also efficient and environmentally friendly. The advent of $LiFePO_4$ electrodes for use in Li^+ ion energy storage devices may fit all necessary criteria. $LiFePO_4$ was one of several candidate materials proposed as an electrode material[1,2], and has received much attention because it has excellent structural and chemical stability during intercalation and thermal cycling, high intercalation voltage of ~3.5 V relative to lithium metal, and high theoretical discharge capacity (~170 mA h g^{-1}).[3–8] $LiFePO_4$ is a naturally occurring mineral,[9] and is relatively benign to the environment, at least compared to some of the typical Li^+ ion cell electrodes. However, this material in its pure form is highly resistive to electrical current, and as such the compound has limited practical applicability. Processes that introduce carbon coatings can appreciably improve the conductivity and discharge capacity of the pure sample while maintaining cost effectiveness.[10,11] An alternative way to significantly increase the conductivity of $LiFePO_4$ is to introduce either Li- or Fe-site dopants;[12–14] Li-site doping in particular has been reported by Chung *et al.* to increase the conductivity of doped $LiFePO_4$ by a factor of 10^8.[12]

This observed phenomenon in doped $LiFePO_4$ has prompted a flurry of theoretical treatments of the band structure of pure $LiFePO_4$ to understand the system's electronic structure more completely. Two of these studies were undertaken by one of this paper's authors,[15,16] with other researchers also taking up this task.[17–19] Although each paper cites results that are unique, the most notable controversy concerns the treatment of electron correlation. All five authors approach the problem using various band structure theories, although they are all based upon density functional theory (DFT). Their results show band gaps between 0 and 1 eV. However, Zhou *et al.*[19] also conduct a study using the more complex DFT+U approach. These calculations predict a band gap of 3.8 eV. Table I summarizes the relevant results from each of the five authors.

The resolution of this dispute requires experimentation that probes the electronic structure of $LiFePO_4$ and $FePO_4$. However, there has been little effort expended on this goal until now. We present here x-ray absorption (XAS) and resonant inelastic x-ray scattering (RIXS) spectra taken from $LiFePO_4$ and $FePO_4$, measured using synchrotron light. The highly tunable nature of synchrotron radiation allows for an element-specific, site- and momentum-selective probe of the local density of states (DOS) of each atom. This sheds further light on the near-Fermi-edge density of states and other properties of the electronic structure of $LiFePO_4$.

II. EXPERIMENT

The spectra for $LiFePO_4$ and $FePO_4$ were measured at beamline 8.0.1 at the Advanced Light Source, Lawrence Berkeley National Laboratory.[20] This beamline uses an undulator for high photon flux; the end station is comprised of a Rowland circle diffraction grating spectrometer with an area-sensitive multichannel plate detector. The experimental geometry is such that the spectrometer is fixed at a 90° angle with respect to the incoming radiation. The sample plate can be rotated to reach angles of incidence within the range of almost 0° to nearly 90°. The resolution of the incident x rays is controlled by the monochromator slits; they were set to have a resolving power $E/\Delta E \approx 4000$ while measuring the XAS spectra. The monochromator resolution was set to $E/\Delta E \approx 700$ for the RIXS experiment. The resolution of the emitted x rays is controlled by the spectrometer, which has a resolving power $E/\Delta E \approx 500$ for this experiment.

All absorption and emission spectra are normalized to the photon flux impinging the sample, which is monitored by the photoelectron current of a highly transparent gold mesh. The Fe $L_{2,3}$ XAS spectra for $LiFePO_4$ and $FePO_4$ are displayed on the top portions of Figs. 1(a) and 1(b), respectively. The RIXS spectra for the samples, measured while exciting through the entire threshold, are displayed on the bottom portion of the same figures. Each RIXS spectrum is labeled with its excitation energy. The two figures also display nonresonant x-ray emission spectroscopy (XES) spectra, which

are the 731.9 and 728.4 eV spectra in the $LiFePO_4$ and $FePO_4$ figures, respectively. All XES and XAS spectra have been calibrated with respect to characteristic emission and absorption energies of the metallic Fe reference sample used in Ref. 21.

III. DISCUSSION AND ANALYSIS

An in-depth analysis of $LiFePO_4$ and $FePO_4$ was accomplished by correlating the experimental loss features to band-to-band transitions predicted by the density of states calculations. This technique makes use of the unique properties of resonant inelastic scattering. RIXS is a one-step scattering process that in the case of a $3d$ inner-shell excitation has the same net transition as optical absorption. However, the electronic excitation that occurs during an RIXS event is the net result of simultaneous, virtual core hole creation and annihilation processes. Because the energy required to create a core hole is unique to each element, one can selectively probe different elements in the same compound.[22] Note that the total energy necessary to complete the net transition is always the same for a given scattering transition. This energy is subtracted from the energy of the photon exciting the atom. Thus, a feature that maintains the same energy separation from the elastic peak, regardless of excitation energy, is an inelastic scattering peak. This peak represents a net electronic transition from the valence band to the unoccupied conduction-band states. The energy loss of such an inelastic scattering peak within a RIXS spectrum quantifies the energy separation between local maxima in the occupied and unoccupied states. With this understanding in mind, the structure in RIXS spectra can be directly compared to theoretical density of states calculations without simulating the full RIXS line shape. Note that there is no core-hole wave function to overlap with and distort the valence states in the final state of a RIXS transition, so the calculated ground-state DOSs remain a valid description of the electronic structure during a RIXS event. Our goal was therefore to identify all inelastic features and match them, if possible, to candidate inner-shell scattering transitions identified in the calculated DOS. For the purposes of this analysis, a candidate inner-shell scattering transition will be defined as a transition that moves a valence electron from a local maximum in the occupied states to a local maximum in the unoccupied states.

The purpose for finding the inelastic features and matching them to inner-shell transitions is to determine which calculated model of $LiFePO_4$, characterized by the band gap, is the more accurate. However, the band gap itself is not a determinable quantity in this study. A larger band gap will result in RIXS transitions that exhibit greater energy loss; however, one cannot say with absolute certainty that the transition with the smallest loss of energy also represents the transition from the highest occupied state to the lowest unoccupied state. The problem is that RIXS transitions can

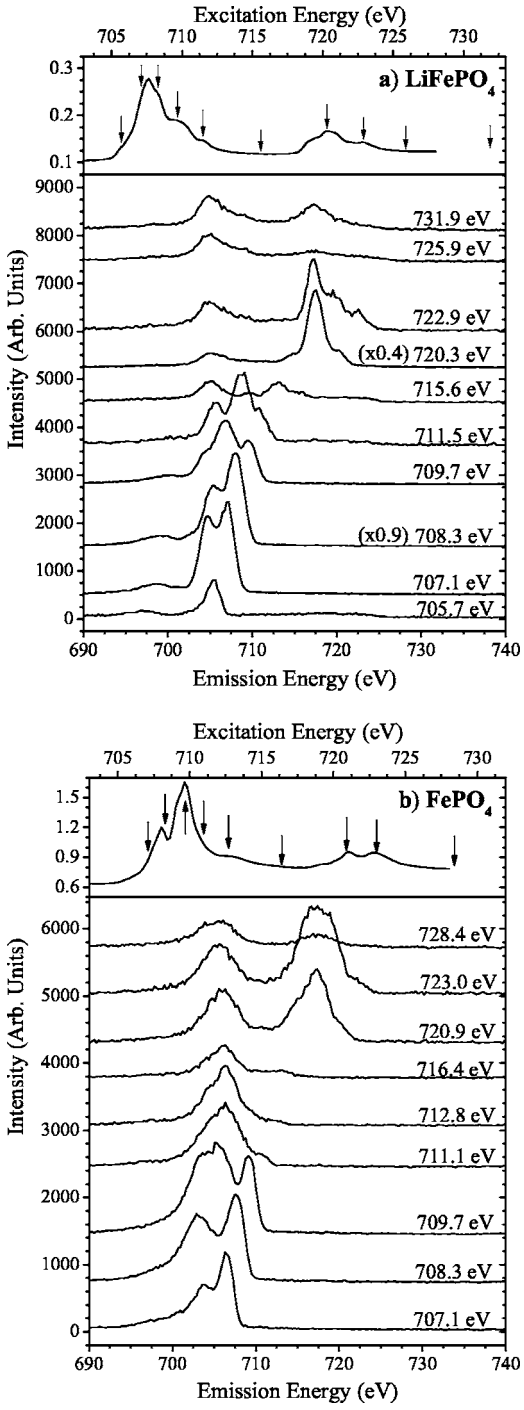

FIG. 1. XAS and RIXS data measured from (a) $LiFePO_4$ and (b) $FePO_4$ displayed on the emission energy axis. Each RIXS spectrum is labeled with its excitation energy. The XAS spectrum for each compound is accompanied by arrows; each indicates the excitation energy for a RIXS spectrum.

TABLE I. Summary of pertinent information taken from other authors.

Author	Correlation?	Band gap (eV)
Xu *et al.* (Refs. 15 and 16)	No	0
Tang and Holzwarth (Ref. 17)	No	0
Shi *et al.* (Ref. 18)	No	1.0
Zhou *et al.* (Ref. 19)	No	0.5
Zhou *et al.* (Ref. 19)	Yes, U=4.3 eV	3.8

have transition probabilities that vary by as much as five orders of magnitude, even though all of them are dipole allowed. As a result, there can be a large number of transitions that will not be detected; one of these undetectable transitions may be the one to bridge the band gap. The result is that studying the band gap using RIXS transitions as the template for tracing the density of states cannot tell us what the band gap is, but rather what the band gap is not. For example, if the lowest energy-loss feature detected is at 2.0 eV below the elastic peak, then one cannot know if the band gap is less than 2.0 eV, but one can conclude that it is not greater than 2.0 eV. Thus, one can impose an upper limit on the value of the band gap, even if it cannot be measured directly.

To find all energy-loss features within the RIXS spectra of $LiFePO_4$ and $FePO_4$, the spectra were fitted to a set of Voigt functions. To the best of our knowledge, this type of analysis is not commonly utilized with RIXS spectra. Voigt peak fitting allows for the identification of all constituent energy-loss features that overlap to form the measured RIXS spectrum. Voigt peaks were chosen because a Voigt function is the convolution of a Gaussian peak and a Lorentzian peak. The mathematical form of the normalized Voigt profile is described as follows:

$$V(x;\sigma,\gamma) = \int_{-\infty}^{\infty} G(x';\sigma)L(x-x';\gamma)dx',$$

where

$$G(x;\sigma) = \frac{1}{\sigma\sqrt{2\pi}} \exp\left(\frac{-(x-x_0)^2}{2\sigma^2}\right),$$

$$L(x;\gamma) = \frac{\gamma}{\mu[(x-x_0)^2+\gamma^2]}.$$

$G(x';\sigma)$ is the Gaussian component with full width at half maximum (FWHM) of 2.354σ, and $L(x-x';\gamma)$ is the Lorentzian component with FWHM of 2γ. The function is centered at x_0. The Gaussian part of the Voigt function represents any broadening due to instrumental effects, while the Lorentzian part will simulate any broadening due to lifetime effects inherent to the system under study. The spectra chosen for the Voigt function fitting were excited near the L_3 edge; these spectra were the 705.7, 707.1, 708.3, 709.7, and 711.5 eV for $LiFePO_4$ and 707.1, 708.3, and 709.7 eV for $FePO_4$. This edge is preferable for fluorescence experiments because nonradiative decay processes, such as Coster-Kronig transitions, are not as significant when exciting on the L_3 edge as when exciting on the L_2 edge.[23] Before Voigt function fitting, all RIXS spectra were smoothed using a second-order Savitsky-Golay function to suppress noise. The experimental spectra are displayed in Fig. 2 before any manipulation, other than to subtract the excitation energy. Figure 2(a) shows the $LiFePO_4$ spectra, whereas Fig. 2(b) shows those spectra from $FePO_4$.

The Voigt peak fitting analysis was performed using the following hierarchy of criteria. First, the fitted curve must reproduce the experimental curve as closely as possible. Second, all Voigt functions used in the fit must maintain a reasonable FWHM with respect to the other peaks in the fit and the experimental spectrum. This is especially necessary for the Gaussian component of the Voigt functions. Since the Gaussian component represents instrumental broadening, this should be constant for all Voigt functions in the fit. This criterion is meant to prevent the addition of extremely narrow or wide peaks that may be mathematically beneficial in reducing the χ^2 value of the fit, but are physically unreasonable. Third, the fit must be reproducible given a reasonable error in the initial placement of the Voigt functions before the iterative fitting process is undertaken. Each time the fitting

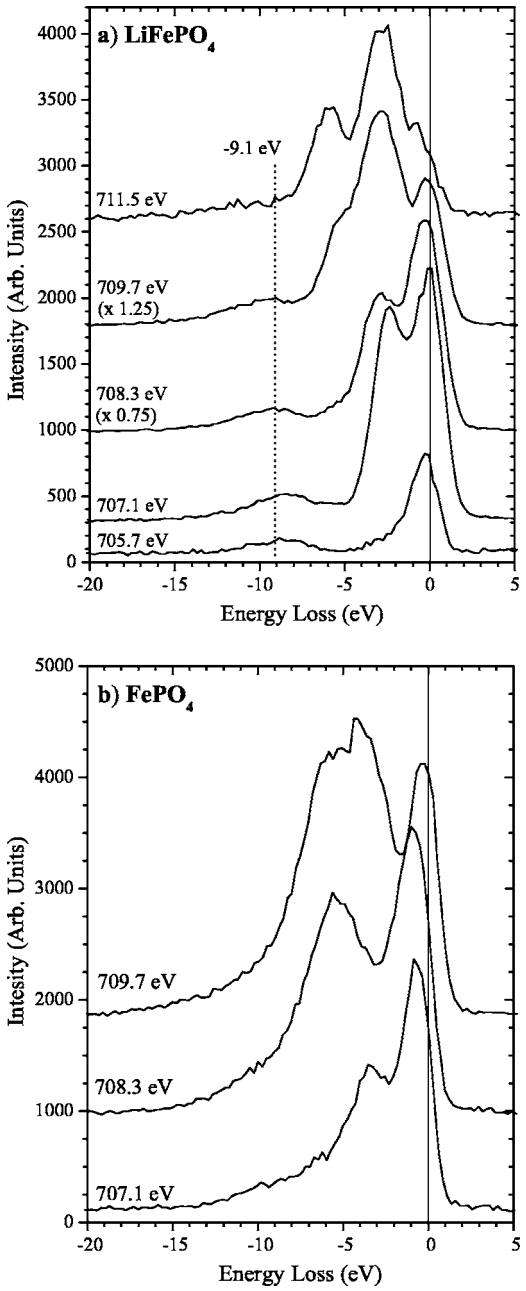

FIG. 2. RIXS spectra on the energy-loss scale for (a) $LiFePO_4$ and (b) $FePO_4$. The solid line represents the excitation (elastic) energy. In (a), the dotted line labeled −9.1 eV is the approximate center of a broad inelastic feature common to all $LiFePO_4$ spectra.

program is given the same number of peaks with roughly the same centers of gravity and FWHM values as inputs, the program should produce the same fit. If this is not the case, there are too many degrees of freedom available to the fitting program.

The results of the Voigt function fits are displayed in Fig. 3 and Tables II and III. Figure 3(a) and Table II pertain to $LiFePO_4$, and Fig. 3(b) and Table III concern $FePO_4$. In Fig. 3, each frame in the figure displays the smoothed experimental spectrum of interest (dotted line), the final fit (solid line), the individual Voigt peaks that constitute the fit, and a difference line that quantifies the difference between the smoothed experimental spectrum and the fit. The difference line is the thicker, dark line displayed at the bottom of each frame. Tables II and III give more precise data for every peak in each fit for $LiFePO_4$ and $FePO_4$, respectively. In the tables, the center of gravity, the total area, and the Lorentzian, Gaussian, and total FWHMs are displayed for each peak in a given fit. The total FWHM is simply the FWHM of the peak that is the superposition of the Lorentzian and Gaussian components.

Recall that one of the guiding criteria used in the creation of the displayed Voigt function fits is that the Gaussian FWHM of each peak should be equal to all other peaks within the fit. In the so-called central region, i.e., that region less than 7.0–8.0 eV below the elastic peak for $LiFePO_4$ and $FePO_4$, this criterion was achieved. Considering the 707.1, 708.3, and 709.7 eV spectra for $LiFePO_4$, the central region had an average Gaussian FWHM of 1.63 eV, with a standard deviation of 0.21 eV. For $FePO_4$, the average was 1.25 eV with a standard deviation of 0.14 eV. However, outside of the central region, the Voigt functions do not exhibit such well-ordered behavior. These Voigt functions include those that are used to describe the broad high-energy loss features in $LiFePO_4$ and $FePO_4$. The Gaussian FWHMs of these features were inconsistently reported among fitting results, which is attributed to the fact that the statistics in the region of −15.0 to −8.0 eV loss are too poor for reproducible results to be achieved. The reason for this will be discussed later. There are also peaks on the positive side of the elastic peak in the 711.5 and 705.7 eV $LiFePO_4$ spectra. Information about these peaks is shown in Table II for completeness, but the peaks are not displayed in Fig. 3(a) because they are not relevant to the discussion of the RIXS features in $LiFePO_4$. These are not real inelastic features due to light scattering from $LiFePO_4$. It is likely that these features are the result of a systematic effect from instrumentation, a problem that is eliminated in the 707.1, 708.3, and 709.7 eV spectra because they were measured at a different time, and they were measured over a longer time interval. These three spectra exhibit better statistics and do not show any sign of these positive side peaks. The unknown contribution of this instrumentation effect is the reason why the FWHMs of the Voigt functions from the 711.5 and 705.7 eV spectra are not included in the FWHM average for $LiFePO_4$.

With the exception of the elastic peaks, the Lorentzian FWHM was not nearly so consistent among the well-defined central region peaks for both materials. Not including the elastic peaks, the Voigt functions for $LiFePO_4$ showed a mean Lorentzian width of 0.72 eV, with a standard deviation

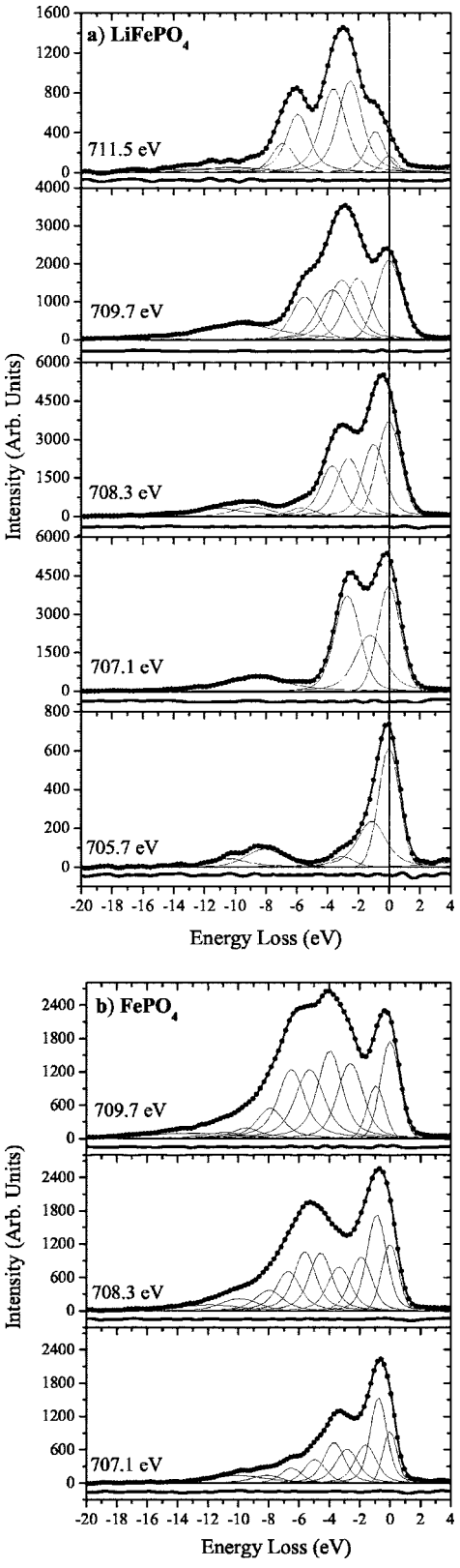

FIG. 3. Peak fitting analysis results for each of the seven selected spectra from (a) $LiFePO_4$ and (b) $FePO_4$. The dotted lines are the experimental spectra after filtering with the second-order-Savitsky-Golay function. The Voigt fit is plotted over the RIXS data. The dark line beneath represents the difference between calculated fit and experimental data.

TABLE II. Voigt peak fitting analysis results for $LiFePO_4$.

Peak no.	Center of gravity	Total FWHM	Gaussian FWHM	Lorentzian FWHM	Integrated area
			Peak data: 711.5 eV spectrum		
1	−12.20	7.00	7.00	0.00	278
2	−10.24	5.64	5.64	0.00	315
3	−6.89	1.68	1.14	0.88	656
4	−5.92	1.78	1.01	1.18	1459
5	−3.61	1.93	1.24	1.11	2188
6	−2.52	1.87	1.22	1.04	2294
7	−0.88	1.40	0.82	0.90	806
8	0.00	1.20	1.20	0.00	213
9	7.45	7.67	7.67	0.00	483
			Peak data: 709.7 eV spectrum		
1	−9.62	6.16	3.67	3.87	3315
2	−5.47	1.98	1.77	0.38	2579
3	−3.68	2.31	1.85	0.79	3704
4	−3.07	2.13	1.59	0.90	4229
5	−2.03	1.96	1.63	0.57	3806
6	0.00	1.94	1.94	0.00	4312
			Peak data: 708.3 eV spectrum		
1	−10.96	3.94	0.33	3.91	1916
2	−8.88	2.93	2.23	1.19	1401
3	−5.67	1.99	1.64	0.62	818
4	−3.69	1.78	1.16	1.00	4713
5	−2.61	1.90	1.46	0.74	5373
6	−0.99	1.75	1.37	0.64	6072
7	0.00	1.80	1.80	0.00	7090
			Peak data: 707.1 eV spectrum		
1	−8.64	4.91	2.37	3.70	3806
2	−2.71	1.95	1.70	0.44	8506
3	−1.23	2.26	1.59	1.10	6436
4	0.00	1.74	1.74	0.00	7650
			Peak data: 705.7 eV spectrum		
1	−10.35	2.84	0.00	2.84	195
2	−8.07	2.91	2.46	0.80	320
3	−3.02	1.76	1.46	0.54	112
4	−1.13	2.19	1.35	1.32	701
5	0.00	1.59	1.59	0.00	1046
6	6.56	7.34	7.34	0.00	278
7	14.19	8.00	8.00	0.00	584

of 0.23 eV; for $FePO_4$, the mean was 0.91 eV with a standard deviation of 0.39 eV. However, consistency of width for the Lorentzian component for energy-loss peaks is not nearly so strict a guideline as for Gaussian broadening. Whereas Gaussian broadening defines the systematic instrumental effects, which should be identical for all inelastic scattering events, the Lorentzian component describes the lifetime broadening, which may vary considerably from peak to peak depending on the stability of the virtual intermediate and final states that make up the net transition. In sharp contrast to the inelastic features, the Lorentzian broadening of every elastic peak was nonexistent for both materials. This is to be expected; a large part of the elastic peaks is simply reflected radiation, which has no lifetime broadening.

Experiment and theory are compared in Fig. 4. Figures 4(a) and 4(b) display the calculated ferromagnetic Fe spin-

TABLE III. Voigt peak fitting analysis results for $FePO_4$.

Peak no.	Center of gravity	Total FWHM	Gaussian FWHM	Lorentzian FWHM	Integrated area
			Peak data: 709.7 eV spectrum		
1	−12.89	6.71	6.71	0.00	684
2	−10.90	2.96	0.00	2.96	508
3	−9.47	2.25	0.00	2.25	682
4	−7.89	2.10	1.18	1.40	1590
5	−6.50	2.08	1.18	1.38	3587
6	−5.29	2.25	1.45	1.28	3737
7	−3.96	1.91	1.14	1.20	4126
8	−2.61	2.00	1.55	0.76	3370
9	−0.93	1.35	1.34	0.02	1366
10	0.00	1.49	1.49	0.00	2771
			Peak data: 708.3 eV spectrum		
1	−11.84	4.68	3.36	2.18	634
2	−9.90	2.90	2.38	0.90	770
3	−7.97	2.15	1.37	1.23	1064
4	−6.70	1.87	1.19	1.09	1799
5	−5.61	1.72	1.07	1.03	2490
6	−4.57	1.77	1.20	0.93	2438
7	−3.35	1.80	1.33	0.79	1814
8	−1.90	1.67	1.37	0.52	1954
9	−0.88	1.51	1.26	0.45	3150
10	0.00	1.32	1.32	0.00	1681
			Peak data: 707.1 eV spectrum		
1	−9.99	4.59	0.00	4.59	1004
2	−8.12	2.34	1.20	1.70	471
3	−6.50	1.63	1.16	0.79	572
4	−4.95	1.64	1.23	0.70	890
5	−3.69	1.64	1.17	0.77	1537
6	−2.83	1.76	1.19	0.93	1411
7	−1.60	1.66	1.24	0.71	1450
8	−0.76	1.30	1.01	0.50	2496
9	0.00	1.09	1.09	0.00	1077

polarized partial density of states for $LiFePO_4$ and $FePO_4$. The figure displays several arrows; these represent $3d$ inner-shell electronic transitions. During such a transition, an electron is scattered from the states indicated by the left arrowhead to the states represented by the right arrowhead. The arrow lengths are the energy values of the centers of gravity of the peaks that constitute the Voigt function simulations shown in Fig. 3. Note that each arrow only denotes a possible transition with the corresponding energy loss. In some cases, such as the 3.0 eV energy-loss feature, there are four possible combinations of initial and final states that can occur, and any or all of the displayed transitions can contribute to the peak measured in the experimental RIXS spectrum.

The analysis clearly shows that the calculated density of states has accurately predicted the relative energy positions of the occupied and unoccupied states. The power of the Voigt function fitting technique is shown through the discovery of the ~ -0.95 and ~ -1.2 eV features, which otherwise were not detectable. With a resolving power of $E/\Delta E \approx 500$, the spectrometer could only resolve peaks that were separated by energies greater than ~ 1.3 eV, thus the -1.2 and -0.95 eV energy-loss features were not visually differentiable from neighboring peaks. However, the inclusion of these peaks in their respective fits was necessary, for both a proper simulation of the spectral line shape and a reasonable Gaussian FWHM for the elastic peak. It would seem, at this point in the analysis of $LiFePO_4$ and $FePO_4$, that the displayed RIXS results support the idea that one does not have to explicitly account for the effects of electron correlation when calculating the band structure of these materials.

Detailed consideration of the experimental and theoretical results for $LiFePO_4$ and $FePO_4$ reveals three issues to con-

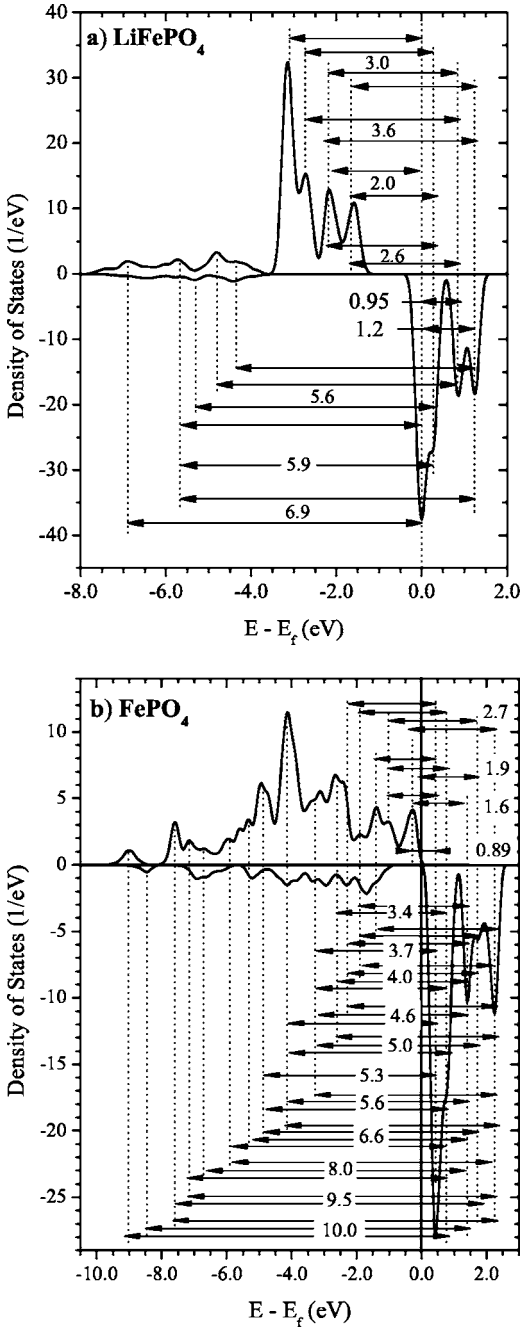

FIG. 4. Fe 3*d* PDOS calculations and assignment of energy losses found during Voigt peak fitting for (a) $LiFePO_4$ and (b) $FePO_4$. Note that because of the delocalized nature of the $FePO_4$ occupied Fe PDOS, the DOS was broadened by 0.3 eV to make it easier to see where lie the points of greatest density.

sider. First, $FePO_4$ RIXS spectra are broader than $LiFePO_4$ spectra at the same energy. The greater broadness of the $FePO_4$ RIXS spectra results from delocalization of the Fe valence electrons due to greater overlap and hybridization of the Fe 3*d* states with neighboring O 2*p* states, as Tang *et al.* first predicted.[17] The greater covalency is due to the inductive effect of the phosphorous sites as suggested by Padhi *et al.*,[1] an effect in which the Fe and P sites compete with one another for the greater share of the bonding with their mutual O site neighbor. The lessened degeneracy of the Fe valence states allows for many possible scattering transitions in the $FePO_4$ RIXS spectra, as is displayed by the greater number of peaks uncovered by Voigt function fitting. This rich structure, when measured with insufficient resolution, blends together to produce the broader line shape that is characteristic of $FePO_4$. Note that the lessened degeneracy of the $FePO_4$ Fe partial density of states (PDOS) is most likely the reason why the Voigt functions in the $FePO_4$ have smaller FWHM than their $LiFePO_4$ counterparts. Recall that the $FePO_4$ spectra had an average Gaussian FWHM of 1.25 eV, which is very close to the resolution of the spectrometer, but the $LiFePO_4$ average Gaussian FWHM was 1.63 eV. The greater energy separation of the states in $FePO_4$ means that every inelastic feature in the RIXS spectra represents only one transition. However, in $LiFePO_4$, the degeneracy is more pronounced, meaning that each inelastic feature is the average of several transitions that are separated by less than 0.1–0.2 eV. Peaks that are separated by such a small energy value cannot be differentiated in the Voigt function fitting process, so the "average" peak that describes the entire group has to be wider to cover all transitions.

The second issue of note concerns the broad feature at approximately −9.1 eV energy loss that appears in all $LiFePO_4$ spectra, as seen in Fig. 2(a). In the 705.7 eV spectrum, this feature is jointly represented by the −10.4 and −8.1 eV Voigt functions. This energy-loss feature is modeled by the peak at −8.6 eV in the 707.1 eV spectrum, by the peaks at −11.0 and −8.9 eV in the 708.3 eV spectrum, by the peak at −9.6 eV in the 709.7 eV spectrum, and finally by the peaks at −12.2 and −10.2 eV in the 711.5 eV spectrum. The feature is much wider than the other energy-loss features shown in Fig. 3(a) and grows ever wider at higher excitation energies. At 709.7 eV, the Voigt function used to model the energy loss feature has a total FWHM of 6.2 eV,which is approaching threefold that of the other peaks. This width covers most of the Fe valence band, and as such this feature cannot be due to a simple 3*d* inner-shell scattering excitation. The feature is the superposition of many transitions that cannot be individually resolved. At higher excitation energies, these transitions become more numerous and increase the overall width of the feature. This is what happens to a lesser extent in $FePO_4$, as discussed above. It is likely that the −9.1 eV feature is the superposition of RIXS transitions from the 3*d* band to the 4*s* band, because the 4*s* band is sufficiently broad. Note that, as displayed in Fig. 5, there are some states in the occupied Fe 3*d* PDOS centered at about −8.5 eV from which electrons could scatter to form the −9.1 eV feature. Indeed, it is entirely possible that there is a 3*d* inner-shell scattering transition occurring at approximately −9.1 eV, and it is simply superimposed on all the other transitions occurring at that energy. However, there is no physically reasonable explanation for why this particular inner-shell transition should give rise to an energy-loss peak whose FWHM departs so strongly from the FWHM of the other inelastic scattering features.

Figure 5 shows the theorized 3*d*-4*s* scattering event in $LiFePO_4$. In order to find the theorized center of the transition to compare to experiment, the centroids for the Fe 3*d* occupied spin-up and spin-down PDOSs and the Fe 4*s* un-

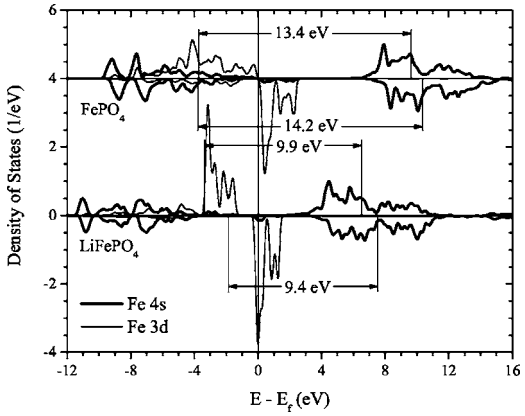

FIG. 5. $LiFePO_4$ and $FePO_4$ Fe 3*d* and 4*s* spin-polarized PDOSs. The dark lines are the 4*s* states, while the thinner lines are the 3*d* states. The 3*d* PDOSs have been divided by 10 so that the 4*s* PDOS would be more prominent. There are four RIXS net transitions displayed, one for each spin direction of $LiFePO_4$ and $FePO_4$ such that $\Delta S=0$ in all cases. In these transitions, electrons are scattered from the 3*d* occupied to the 4*s* unoccupied states.

occupied spin-up and spin-down PDOSs were calculated. Since there are an equal number of states to either side of the centroid, the energy separating the centroids should reflect the approximate center of the transition in question. This centroid separation energy turns out to be between 9.9 and 9.4 eV for the spin-up and spin-down channels, respectively, which places it 0.3–0.8 eV over the measured −9.1 eV center. This error, however, is not unexpected. Both the spin-up and spin-down 3*d* occupied bands are highly asymmetric about their centroids, so all low-energy-loss transitions scattered from the near-Fermi-edge states will be narrower and higher than the high-energy-loss transitions scattered from deeper states. The asymmetric shape of the 3*d* band causes the highest point in the 3*d*-4*s* scattering feature to be skewed to lower values of energy loss in the experimental spectrum. This asymmetry also prevents an accurate simulation of the −9.1 eV feature with a single Voigt function. The incorrect centers of gravity of the Voigt functions used to reproduce the −9.1 eV feature in the 707.1, 708.3, 709.7, and 711.5 eV fits represent the best simulation of the asymmetric experimental line shape. $FePO_4$ is included in Fig. 5 as well, as there are peaks at high energy loss that have large FWHM that may be the result of 3*d*-4*s* scattering. However, no conclusions have been drawn concerning $FePO_4$ because accurate representations of the $FePO_4$ spectra below −7.0 eV energy loss could not be reproducibly obtained.

The third and final issue of note concerns the intensity of the −5.6 eV loss feature compared to the intensity of the −3.0 eV loss feature in the $LiFePO_4$ 709.7 eV spectrum. The −3.0 eV feature has four possible transitions contributing to its strength; in each transition, electrons are scattered from the densest part of the Fe 3*d* occupied spin-up PDOS. The −5.6 eV scattering event also has four possible transitions, but the occupied states are more sparsely populated. The −3.0 eV transition has 360% more occupied states from which electrons may be scattered, yet the measured −3.0 eV peak is only 64% more intense than the −5.6 eV peak. Obviously, the RIXS transition probability matrix elements for the two events are grossly unequal. This inequality is due to the involvement of the spin-down occupied states that help give rise to the −5.6 eV energy-loss feature.

Strictly speaking, the selection rules for RIXS state that $\Delta S=0$. Thus, during any scattering event that begins with the 3*d* occupied spin-up states, the scattered electron must flip its spin before coming to rest in the spin-down unoccupied states. At finite temperatures, this can be accomplished via magnon-exciton coupling.[24–27] This concept has been used extensively to explain the presence of dipole-allowed peaks in optical absorption spectra. Optical absorption and RIXS share the same 3*d* inner-shell net transition, and like RIXS, dipole-allowed peaks in optical absorption spectra must also obey the $\Delta S=0$ spin selection rule. Magnon-exciton coupling allows the electron component of the exciton pair to couple with a magnon, thus flipping the spin of the electron. At room temperature, the magnon can be a randomly generated event from heat-induced fluctuations. In antiferromagnetic systems, however, the magnon can be deliberately produced through interaction of the magnetic atom being excited by the incoming radiation and another magnetic atom on a neighboring antiparallel magnetic plane. Either way, transitions that require this mechanism to flip the spin of the excited electron, such as the −3.0 eV transition, rely upon the presence of another particle. Thus the probability that the transition will happen suffers in comparison to a transition that does not require an external mechanism to flip the electron's spin, such as the −5.6 eV transition. Therefore, magnon-exciton coupling provides the means by which the −3.0 eV transition may occur while simultaneously causing the rate-determining step that limits the probability that the transition will occur. The fact that the −5.6 and −3.0 eV features are of comparable size is further evidence that the DOSs presented in this paper are accurate, as the DOS provides a physically reasonable explanation why the −5.6 eV loss is so intense despite the hindrance of low density in the electron's source states.

IV. COMPARISON OF THEORETICAL MODELS

Thus far we have shown that the RIXS data for both $LiFePO_4$ and $FePO_4$ agree extremely well with the PDOSs calculated for these systems. However, the quality of agreement between theory and experiment for $LiFePO_4$ is surprising, for two reasons. First, the Fe PDOSs displayed in Figs. 4 and 5 assumed $LiFePO_4$ to be ferromagnetic, because the ferromagnetic solution was energetically favorable. This contradicts the experimental evidence that the compound is antiferromagnetic in its ground state.[28,29] Second, the theory that produced the DOS for $LiFePO_4$ and $FePO_4$ was the local density approximation (LDA)-based orthogonalized linear combination of atomic orbitals (OLCAO) regimen, which does not explicitly take into account electron correlation effects that cause the large band gaps and insulating behavior demonstrated by many transition metal oxides. As stated in the Introduction, there is a debate in the literature as to how to correctly treat these materials, with the argument centering on the question of electron correlation.

Both sides of the debate (correlated vs uncorrelated functionals) have the support of experimental evidence. To support the uncorrelated DOS, there is the evidence presented in this paper, wherein the presented RIXS spectra and DOS match extremely well. There is also the fact that Xu *et al.*[15] measured an activation energy of 0.36 to 0.50 eV, which fits best with the small-band-gap solutions. Despite the low activation energy, $LiFePO_4$ has extremely poor conductivity, which is typically characteristic of a wide-gap insulator. This supports the solution that incorporates electron correlation effects. Also, optical reflectance measurements presented in the same paper as the wide-gap DOS show that the band gap is on the order of 3.8–4.0 eV, in accordance with their predicted result. It should be noted, however, that the lowest energy that is displayed in the optical reflectance spectrum is on the order of 2 eV. Although the spectrum is strong evidence for the wide-gap solution, it does not rule out the possibility that a structure near 0.5 eV was simply missed. Finally, in another paper, Zhou *et al.* showed that LDA-based techniques predict that off-stoichiometric samples of $LiFePO_4$, such as $Li_{0.7}FePO_4$, have a negative energy of formation.[30] This would suggest that off-stoichiometric samples should spontaneously form; however, this is known to be untrue. An incomplete delithiation of $LiFePO_4$ will result in a multiphase compound with zones of $LiFePO_4$ and $FePO_4$ spread throughout the sample. It would seem that the two mutually exclusive scenarios are both accurate.

In an attempt to solve this conundrum, Zhou and coworkers suggested that the principal conduction mechanism in $LiFePO_4$ was polaronic in nature. We suggest here a variation on this idea: a bound magnetic polaron, or possibly a ferron, defines the conductivity. Originally used to account for surprisingly high values of magnetic susceptance in antiferromagnetic samples, bound magnetic polarons are capable of changing the local magnetic environment from antiferromagnetic to ferromagnetic.[31–35] This alteration of the immediate environment causes the conduction electron to become self-trapped, thus severely limiting conduction despite the low activation energy; ferrons have been suggested as the mechanism that hinders conductivity in some antiferromagnetic semiconductors. This idea is intriguing because the ferromagnetic ground state seems to be, in some formalisms, energetically advantageous, although only slightly. This small difference between ferromagnetic and antiferromagnetic alignment may mean that it is relatively easy for conduction electrons to realign the local environment.

This effect is not limited to low temperatures. Ferrons have been predicted to exist at high temperatures even after random fluctuations have mostly destroyed the magnetic ordering of the compound.[34] The bound magnetic polaron effect suggested here and the simple polaron effect suggested by Zhou *et al.* are phenomena that are catalyzed by the presence of impurities.[36] This suggests that $LiFePO_4$ is extremely sensitive to impurity concentration, but this is not a new realization; $LiFePO_4$ has already been proven to be dopant sensitive by previous efforts.

V. CONCLUSIONS

We have probed $LiFePO_4$ and $FePO_4$ using XAS and RIXS techniques. We have found via Voigt peak fitting analysis that the energy-loss features seen in the RIXS spectra correspond very well to Fe $3d$ inner-shell valence to conduction-band transitions, as predicted by the presented DOS calculations. This contradicts the more accurate DFT $+U$ calculations presented in the literature. However, optical absorption measurements have shown the band gap of the sample to be 3.8–4.0 eV wide. We have tentatively explained that our experimental spectra result from the effect of a bound magnetic polaron, which would distort the local PDOS and cause a local ferromagnetic environment to form around the excited conduction electron. The existence of the bound magnetic polaron is a strong impurity effect that may not be present in all samples of $LiFePO_4$. The formation of such an effect may depend upon the method of synthesis.

ACKNOWLEDGMENTS

Funding by the Natural Sciences and Engineering Research Council of Canada (NSERC) and the Canada Research Chair program is gratefully acknowledged. Wai-Yim Ching acknowledges funding by U.S. DOE under Grant No. DE-FG02-84DR45170.

[1] A. K. Pahdi, K. S. Nanjundaswamy, and J. B. Goodenough, J. Electrochem. Soc. **144**, 1188 (1997).
[2] G. Ceder, Y.-M. Chiang, D. R. Sadoway, M. K. Aydinol, Y.-I. Jang, and B. Huang, Nature (London) **392**, 694 (1998).
[3] A. Yamada, S. C. Chung, and K. Hinokuma, J. Electrochem. Soc. **148**, A224 (2001).
[4] A. S. Andersson, J. O. Thomas, B. Kalska, and L. Häggström, Electrochem. Solid-State Lett. **3**, 66 (2000).
[5] A. Deb, U. Bergmann, E. J. Cairns, and S. P. Cramer, J. Phys. Chem. B **108**, 7046 (2004).
[6] S. Yang, Y. Song, K. Ngala, P. Y. Zavalij, and M. S. Whittingham, J. Power Sources **119–121**, 239 (2003).
[7] M. Takahashi, H. Ohtsuka, K. Akuto, and Y. Sakurai, J. Electrochem. Soc. **A899-A904**, 152 (2005).
[8] M. Takahashi, S. Tobishima, K. Takei, and Y. Sakurai, J. Power Sources **97–98**, 508 (2001).
[9] N. Ravet, Y. Chouinard, J. F. Magnan, S. Besner, M. Gauthier, and M. Armand, J. Power Sources **97–98**, 503 (2001).
[10] K. Amine, J. Liu, and I. Belharouak, Electrochem. Commun. **7**, 669 (2005).
[11] C. H. Mi, G. S. Cao, and X. B. Zhao, Mater. Lett. **59**, 127 (2005).
[12] S.-Y. Chung, J. T. Bloking, and Y.-M. Chiang, Nat. Mater. **1**, 123 (2002).
[13] S. Shi, L. Liu, C. Ouyang, D.-S. Wang, Z. Wang, L. Chen, and X. Huang, Phys. Rev. B **68**, 195108 (2003).
[14] D. Wang, H. Li, S. Shi, X. Huang, and L. Chen, Electrochim. Acta **50**, 2955 (2005).
[15] Y.-N. Xu, S.-Y. Chung, J. T. Bloking, Y.-M. Chiang, and W.-Y.

Ching, Electrochem. Solid-State Lett. **7**, A131 (2004).
[16] Y.-N. Xu, W.-Y. Ching, and Y.-M. Chiang, J. Appl. Phys. **95**, 6583 (2004).
[17] P. Tang and N. A. W. Holzwarth, Phys. Rev. B **68**, 165107 (2003).
[18] S. Shi, C. Ouyang, Z. Xiong, L. Liu, Z. Wang, H. Li, D.-S. Wang, L. Chen, and X. Huang, Phys. Rev. B **71**, 144404 (2005).
[19] F. Zhou, K. Kang, T. Maxisch, G. Ceder, and D. Morgan, Solid State Commun. **132**, 181 (2004).
[20] J. J. Jia, T. A. Callcott, J. Yurkas, A. W. Ellis, F. J. Himpsel, M. G. Samant, J. Stöhr, D. L. Ederer, J. A. Carlisle, E. A. Hudson, L. J. Terminello, and D. K. Shuh, Rev. Sci. Instrum. **66**, 1394 (1995).
[21] A. Moewes, E. Z. Kurmaev, L. D. Finkelstein, A. V. Galakhov, S. Gota, M. Gautier-Soyer, J. P. Rueff, and C. F. Hague, J. Phys.: Condens. Matter **15**, 2017 (2003).
[22] P. L. Cowan, in *Resonant Anomalous X-ray Scattering: Theory and Applications*, edited by G. Materlik, C. J. Sparks, and K. Fischer (Elsevier Science Pub. Co., San Diego, CA, 1994), p. 449.
[23] E. Z. Kurmaev, A. L. Ankudinov, J. J. Rehr, L. D. Finkelstein, P. F. Karimov, and A. Moewes, J. Electron Spectrosc. Relat. Phenom. **148**, 1 (2005).
[24] R. J. Elliot, M. F. Thorpe, G. F. Imbusch, R. Loudon, and J. B. Parkinson, Phys. Rev. Lett. **21**, 147 (1968).
[25] S. Freeman and J. J. Hopfield, Phys. Rev. Lett. **21**, 910 (1968).
[26] R. S. Meltzer, M. Y. Chen, D. S. McClure, and M. Lowe-Pariseau, Phys. Rev. Lett. **21**, 913 (1968).
[27] M. F. Thorpe, Phys. Rev. Lett. **23**, 472 (1969).
[28] R. P. Santoro and R. E. Newnham, Acta Crystallogr. **22**, 344 (1967).
[29] G. Rousse, J. Rodriguez-Carvajal, S. Patoux, and C. Masquelier, Chem. Mater. **15**, 4082 (2003).
[30] F. Zhou, C. A. Marianetti, M. Cococcioni, D. Morgan, and G. Ceder, Phys. Rev. B **69**, 201101(R) (2004).
[31] T. Kasuaya, A. Yanase, and T. Takeda, Solid State Commun. **8**, 1543 (1970).
[32] T. Kasuaya, Solid State Commun. **8**, 1635 (1970).
[33] A. Mauger and D. L. Mills, Phys. Rev. B **31**, 8024 (1985).
[34] E. L. Nagaev, Phys. Rev. B **60**, R6984 (1999).
[35] I. Gonzalez, J. Castro, D. Baldomir, A. O. Sboychakov, A. L. Rakhmanov, and K. I. Kugel, Physica B **359-361**, 1418 (2005).
[36] I. G. Austin and N. F. Mott, Adv. Phys. **50**, 757 (2001).